JOURNAL OF COMPUTATIONAL PHYSICS 53, 209–226 (1984)

Finite Analytic Numerical Method for Unsteady Two-Dimensional Navier–Stokes Equations

CHING-JEN CHEN*

AND

HAMN-CHING CHEN†

Energy Division and Iowa Institute of Hydraulic Research, University of Iowa, Iowa City, Iowa 52242

Received June 2, 1982; revised December 16, 1982

The main purpose of this paper is to develop a finite analytic (FA) numerical solution for unsteady two-dimensional Navier–Stokes equations. The FA method utilizes the analytic solution in a small local element to formulate the algebraic representation of partial differential equations. In this study the combination of linear and exponential functions that satisfy the governing equation is adopted as the boundary function, thereby improving the accuracy of the finite analytic solution. Two flows, one a starting cavity flow and the other a vortex shedding flow behind a rectangular block, are solved by the FA method. The starting square cavity flow is solved for Reynolds numbers of 400, 1000, and 2000 to show the accuracy and stability of the FA solution. The FA solution for flow over a rectangular block ($H \times H/4$) predicts the Strouhal number for Reynolds numbers of 100 and 500 to be 0.156 and 0.125. Details of the flow patterns are given. In addition to streamlines and vorticity distribution, rest-streamlines are given to illustrate the vortex motion downstream of the block.

I. INTRODUCTION

When a differential equation cannot be solved analytically, numerical methods are employed. Most of the numerical methods, including the present finite analytic (FA) method, bear the following similarities. First, all methods decompose the total region governed by differential equations into a number of small elements or grid points, and then replace the continuous solution of the differential equation with discrete values at grid points of elements. Second, all methods derive an algebraic equation from the differential equation with suitable difference approximations or suitable profile functions of dependent variables between nodal points. Third, the resulting system of algebraic equations is solved with proper boundary and initial conditions to obtain the numerical solution for all of the grid points. The numerical methods are generally

* Professor.
† Visiting Assistant Professor.

0021-9991/84 $3.00

distinguished by how the corresponding algebraic representation of the differential equation is derived. Several commonly used methods in deriving the discrete algebraic equation in the finite difference method are Taylor-series expansion and control volume (or flux, or box) formulation. For the finite element method, the variational formulation and method of weighted residuals are often used. The finite analytic method presented by Chen *et al.* [1–4] invokes another means of deriving the algebraic equations. Unlike finite-difference or finite-element methods, the discrete algebraic equation is obtained from the analytic solution for each local element in the finite analytical method. This paper presents the development of finite analytic (FA) numerical method to solve unsteady two-dimensional Navier–Stokes equations.

In fluid flow and heat transfer problems, certain difficulties, such as numerical instability and slow convergence, are encountered in solving Navier–Stokes equations or convective transport equations when convective terms are significant. In the finite difference formulation, the difficulty of numerical instability is overcome by considering a central difference approximation for the diffusion term and a backward (upwind) difference for the convective term [5, 6]. Spalding [6] improved the upwind difference by utilizing the exact solution for the steady one-dimensional transport equation to derive an exponential scheme. Patankar [7] developed an approximation called the power-law scheme and used it extensively in the control volume formulation of 2D and 3D unsteady convective transport problems. While the numerical instability can be avoided by the generation of exponential or similar schemes, serious false diffusion may occur, as shown by Patankar [7], when the flow is skewed to the grid lines, and when there is a nonzero gradient of the dependent variables in the direction normal to the flow. This false numerical diffusion is due to an improper approximation of the differential equation by an algebraic expression. In Navier–Stokes equations it is the convective term that creates difficulties.

In finite element formulation, a similar "upwind scheme" was derived recently by Heinrich *et al.* [8], improving the weighting function of standard Galerkin formulation with modifying functions and a set of optimal parameters. The exact solution in one-dimensional cases is recovered in this approach when the optimal parameters are used, and the same optimum parameter can be employed to derive a 9-point formula for the 2D convective transport equation. The 9-point formula thus obtained provides a gradual shift to upwind when the convective velocity on the windward is significant. However, Gallagher *et al.* [9] showed that in both diffusive ($\mathrm{Re} \ll 1$) and convective ($\mathrm{Re} \gg 1$) dominant limiting cases, the resulting 9-point formula does not give physically reasonable asymptotic behaviors. Besides, when unequal grid size is considered, the result may become increasingly unreasonable.

In previous finite analytic formulations, the local analytic solution for the steady convective transport equation in a small element was obtained by Chen *et al.* [1–4] for locally linearized governing equations. They adopted the second-order polynomial to approximate the boundary condition for all boundaries in each small element and showed that the finite analytic solution, by virtue of its analytic nature, can properly account for the influence of the skewed convective vector and the magnitude of the convection. In this report the FA solution for Navier–Stokes equations are further

modified by considering the boundary approximation function to be a combination of exponential and linear functions which are solutions of the governing equation. Furthermore, the FA solution is extended to include unsteady flows. As an application the FA method was first tested for prediction of unsteady flow in a two-dimensional cavity and then applied to solve the flow over a rectangular obstacle behind which vortex shedding occurs.

II. The Finite Analytic Method

The basic idea of the FA method is the incorporation of analytic solutions in the numerical solution of partial differential equations. To illustrate the basic principle of the FA method we consider a partial differential equation (PDE) $L\phi = f$, where L is a linear or nonlinear partial differential operator and f is an inhomogeneous term that depends on the independent variables, such as x, y, and t. The PDE is to be numerically solved with proper boundary and initial conditions. In the FA method the problem is first subdivided into small elements. For example, a typical element, $2h \times 2k$, in a given time interval $\Delta t = t^k - t^{k-1}$ is shown in Fig. 1, where a node $p(i,j)$ at given time t^k or t^{k-1} is surrounded by neigboring node points EC (east center), WC (west center), SC (south center), NC (north center), NE (northeast), NW (northwest), SE (southeast), and SW (southwest). In general, the subscript EC corresponds to $(i+1,j)$. Once the problem is subdivided into small elements, an analytic solution for the PDE in each element may be obtained.

In cases where the PDE is nonlinear, such as the Navier–Stokes equations, the nonlinear equation may be locally linearized in each element. In this fashion the overall nonlinear effect can still be approximately preserved by assembly of local analytic solutions. For example, we consider the incompressible two-dimensional Navier–Stokes equations cast in the dimensionless streamfunction-vorticity formulation

$$\mathrm{Re}\,(\xi_t + (u\xi)_x + (v\xi)_y) - (\xi_{xx} + \xi_{yy}) = 0, \tag{1}$$

$$\nabla^2 \psi = -\xi, \tag{2}$$

$$u = \psi_y, \qquad v = -\psi_x, \qquad \xi = v_x - u_y. \tag{3}$$

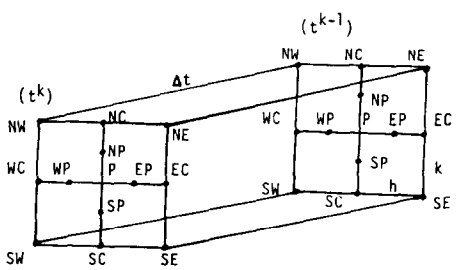

FIG. 1. Finite analytic element.

Here space and time variables (x, y, t) are dimensionless and normalized by a reference length quantity H and a reference time quantity H/U_0. The velocities u and v are normalized by the reference velocity U_0. The Reynolds number is $\mathrm{Re} = U_0 H/v$, velocities u and v are normalized by the reference velocity U_0. To linearize the Navier–Stokes equations in an element we let

$$u = u_p + u', \qquad v = v_p + v', \qquad 2A = \mathrm{Re}\, u_p, \qquad 2B = \mathrm{Re}\, v_p, \tag{4}$$

where u_p and v_p are the velocity components at node p, the deviation of the velocity components in the element from that at node p are u' and v', respectively. They are in general small if the element is reasonably small but can become significant when multiplied by the Reynolds number. Equation (1) under this approximation can be written as

$$2A\xi_x + 2B\xi_y - \xi_{xx} - \xi_{yy} = -\mathrm{Re}[(u'\xi)_x + (v'\xi)_y + \xi_t] = f. \tag{5}$$

If the right side f is considered to be a constant in an element, then a simple analytic solution can be obtained for Eq. (5) at time t^k when proper boundary conditions are specified or

$$\xi = \mathrm{fn}(\xi_N(x), \xi_S(x), \xi_E(y), \xi_W(y), h, k, x, y, t, f), \tag{6}$$

where ξ_N, ξ_S, ξ_E and ξ_W are the northern, southern, eastern, and western boundary conditions, respectively, for the element $2h \times 2k$ at t^k.

For numerical purposes the boundary conditions ξ_N, ξ_S, ξ_E, and ξ_W may be specified in terms of nodal values along the boundary, e.g., $\xi_S = \mathrm{fn}(\xi_{SE}, \xi_{SC}, \xi_{SW}, x)$. Substituting the boundary condition into Eq. (6) and evaluating it at the point $p(i, j)$ at time t^k, one has the finite analytic algebraic formula for the interior nodal ξ_p as

$$\xi_p = C_{EC}\xi_{EC} + C_{WC}\xi_{WC} + \cdots + C_{SW}\xi_{SW} + C_{SE}\xi_{SE} + C_p f_p. \tag{7}$$

Here C's are known analytic coefficients multiplying the corresponding boundary nodal values ξ_{EC} etc., and the particular solution f_p representing the right side of Eq. (5). The system of algebraic equations thus generated for all elements can be solved using the proper boundary conditions of the problem and will provide the FA solution for vorticity distribution. Similarly, Eq. (2) for stream function can be solved likewise by deriving the corresponding finite analytic representation with proper boundary conditions. This is the essence of the FA method.

III. Finite Analytic Solution

In this section we derive the local analytic solutions for the unsteady two-dimensional Navier–Stokes equations cast in stream functions and vorticity formulation, as given in Eqs. (1)–(3). In order to derive an analytic solution in an

element, as shown in Fig. 1, we linearize Eq. (1) as given in Eq. (5). The ellipticity of Eq. (5) in space requires that the boundary conditions ξ_N, ξ_S, ξ_W, and ξ_E be specified. Although many approximate functions can be used to approximate the boundary condition where three nodal values are available for each boundary, it is best to choose the approximate function from the class functions that satisfies the governing equation. For Eq. (5) one finds that a constant, a linear function $(Ay - Bx)$, and an exponential function, $\exp(2Ax + 2By)$, satisfy the homogeneous part of Eq. (5). These functions can be considered as natural or basic modes of the solution form for Eq. (5) out of many other possible forms. Thus, for example, the western boundary condition of the vorticity transport Eq. (5) may be approximated by

$$\xi_W(y) = a_0 + a_1 y + a_2(e^{2By} - 1), \tag{8}$$

where the constants a_0, a_1, and a_2 can be specified by the three nodal values of vorticity on the boundary, namely,

$$\begin{aligned} a_0 &= \xi_{WC}, \\ a_1 &= \frac{1}{2k}\left[\xi_{NW} - \xi_{SW} - \coth Bk(\xi_{NW} + \xi_{SW} - 2\xi_{WC})\right], \\ a_2 &= (\xi_{NW} + \xi_{SW} - 2\xi_{WC})/(4\sinh^2 Bk). \end{aligned} \tag{9}$$

The boundary condition for the north, south, and east sides, i.e., ξ_N, ξ_S, and ξ_E, can be similarly approximated.

Equation (5) with boundary conditions ξ_W, ξ_S, ξ_N, and ξ_E, specified by the eight boundary nodal values, can then be solved analytically by the method of separation of variables. In this investigation the inhomogeneous term, f, of Eq. (5), which contains the perturbation term of convection and unsteady term, is treated as a known constant. When the analytic solution is evaluated at the interior node $p(i,j)$ of the element at time t^K, we have Eq. (7) with the finite analytic coefficients C_{EC}, etc., as

$$\begin{aligned} C_{EC} &= EBe^{-Ah}, & C_{NE} &= Ee^{-Ah-Bk}, \\ C_{WC} &= EBe^{Ah}, & C_{NW} &= Ee^{Ah-Bk}, \\ C_{SC} &= EAe^{Bk}, & C_{SE} &= Ee^{-Ah+Bk}, \\ C_{NC} &= EAe^{-Bk}, & C_{SW} &= Ee^{Ah+Bk}, \end{aligned} \tag{10}$$

$$\begin{aligned} C_p = {} & \frac{Ah}{2(A^2+B^2)}\left[C_{NW} + C_{WC} + C_{SW} - C_{NE} - C_{EC} - C_{SE}\right| \\ & + \frac{Bk}{2(A^2+B^2)}\left[C_{SW} + C_{SC} + C_{SE} - C_{NW} - C_{NC} - C_{NE}\right|, \end{aligned} \tag{11}$$

where

$$E = \frac{1}{4\cosh Ah \cosh Bk} - Ah\,E_2 \coth Ah - Bk\,E_2' \coth Bk$$

$$EA = 2Ah \frac{\cosh^2 Ah}{\sinh Ah} E_2, \qquad E_2 = \sum_{m=1}^{\infty} \frac{-(-1)^m (\lambda_m h)}{[(Ah)^2 + (\lambda_m h)^2]^2 \cosh \mu_m k}, \tag{12}$$

$$EB = 2Bk \frac{\cosh^2 Bk}{\sinh Bk} E_2', \qquad E_2' = \sum_{m=1}^{\infty} \frac{-(-1)^m (\lambda_m h)}{[(Bk)^2 + (\lambda_m' k)^2]^2 \cosh \mu_m' h}, \tag{13}$$

$$\lambda_m = (A^2 + B^2 + \mu_m^2)^{1/2}, \qquad \mu_m = \frac{(2m-1)\pi}{2h},$$

$$\lambda_m' = (A^2 + B^2 + \mu_m'^2)^{1/2}, \qquad \mu_m' = \frac{(2m-1)\pi}{2k}. \tag{14}$$

A relationship between E_2 and E_2' can be found to be

$$h^2 E_2 - k^2 E_2' = \frac{Bh \tanh Ah - Ak \tanh Bk}{4AB \cosh Ah \cosh Bk}. \tag{15}$$

The evaluation of the inhomogeneous term f_p, which contains the unsteady term and the perturbed convection term, is

$$(\xi_t)_p = (\xi_p^k - \xi_p^{k-1})/\Delta t, \tag{16}$$

$$\begin{aligned} F_p &= \mathrm{Re}[(u'\xi)_x + (v'\xi)_y] \\ &= \mathrm{Re}[(u_{EC} - u_p)\,\xi_{EP} - (u_{WC} - u_p)\,\xi_{WP}]/2h \\ &\quad + \mathrm{Re}[(v_{NC} - v_p)\,\xi_{NP} - (v_{SC} - v_p)\,\xi_{SP}]/2k, \end{aligned} \tag{17}$$

where EP, WP, NP, SP, as shown in Fig. 1, denotes the nodes located $\pm h/2$ and $\pm k/2$ from the node P. The values of ξ_{EP}, ξ_{WP}, ξ_{NP} and ξ_{SP} can be evaluated from a similar approximation function used in the boundary approximation like Eq. (8).

Substituting Eqs. (16) and (17) for f_p in Eq. (10) one has

$$\xi_p^k = \left[\sum_{n=1}^{8} C_n \xi_n^k - C_p F_p^{k-1} + \frac{C_p \mathrm{Re}\,\xi_p^{k-1}}{\Delta t}\right] \Big/ \left(1 + \frac{C_p \mathrm{Re}}{\Delta t}\right), \tag{18}$$

where n denotes the boundary nodes EC, NE, NC, etc.

In general the finite analytic coefficient, C_{NE}, C_{EC}, etc., are functions of local cell Reynolds number $2Ah$ and $2Bk$ which are different from one element to another due to the locally linearized velocity u_p and v_p and the grid sizes h and k which vary from element to element. Two typical FA solutions of Eq. (7) with $f = 0$ and $h = k$ are

schematically illustrated in Eqs. (19) and (20) for two different convective vectors and Reynolds numbers,

$$(2Ah = 10) \quad \xi_p = \begin{array}{|c|c|c|} \hline 2 \times 10^{-5} & 1 \times 10^{-5} & 10^{-9} \\ \hline 0.23854 & (P) & 1 \times 10^{-5} \\ \hline 0.52286 & 0.23854 & 2 \times 10^{-5} \\ \hline \end{array} \times \xi_n, \qquad (19)$$

$$(2Bk = 10)$$

$$(2Ah = 100) \quad \xi_p = \begin{array}{|c|c|c|} \hline 0.01 & 10^{-11} & 10^{-48} \\ \hline 0.98 & (P) & 10^{-44} \\ \hline 0.01 & 10^{-11} & 10^{-48} \\ \hline \end{array} \times \xi_n. \qquad (20)$$

$$(2Bk = 0)$$

In Eqs. (19) and (20) the value in the block is the FA coefficient of the corresponding node to be multiplied by the nodal value ξ_n. The summation of these products provides the FA coefficient of ξ_p for the element given in Eq. (7). These FA coefficients can be interpreted as the percentage influence of the boundary node ξ_n on the interior node ξ_p under the given convective vector with components of $2Ah$ and $2Bk$. Equation (19) shows that when the convection comes from the southwest corner with cell Reynolds number of $2Ah = 2Bk = 10$, the FA analytic solution predicts that the influence of the southwest boundary node, ξ_{SW}, on the interior node ξ_p will be the strongest, while the downstream node, NE, has practically zero influence at 10^{-9}. On the other hand Eq. (20) shows that when the convection comes directly from the west side with large cells Reynolds number, the influence of the WC node on the p node is at a dominant strength of 98%, while the other two upwind nodes, NW and SW, are merely 1%. The other boundary nodes are effectively negligible at this high cell Reynolds number. These two examples illustrate that the FA solution can properly predict with analytic means the influence of the boundary node on the determination of the interior node ξ_p with any skewed convective vector and magnitude. This is a distinct feature of the FA method.

When the vorticity function is known, the stream function can be solved from Eq. (2). The finite analytic solution of stream function in an element $2h \times 2k$ can be easily obtained if one notes that Eq. (2) is a special case of Eq. (5). By replacing ξ by ψ and f by ξ in Eq. (7) and letting $A = B = 0$, one has the analytical algebraic representation of stream function ψ_p at the node p as

$$\psi_p = \sum_{n=1}^{8}{}' C'_n \psi_n + C'_p \xi_p. \qquad (21)$$

Here C'_n and C'_p are finite anlaytic coefficients given in Eqs. (10) and (11) with $A = B = 0$. Furthermore, these FA coefficients, because of $A = B = 0$, are invariant. For example, with $h = k$, $C'_{EC} = C'_{WC} = C'_{NC} = C'_{SC} = 0.205315$, $C'_{NE} = C'_{NW} = C'_{SE} =$

$C'_{SW} = 0.044685$, and $C'_p = 0.294685h^2$. Equations (18) and (21) are solved by a line-by-line method in the calculation. For Eq. (21) an overrelaxation factor of 1.6 was used in the iteration, while for Eq. (18), no relaxation is needed since a time-marching procedure is adopted. In the computation, the only summation term that needs to be evaluated numerically is E_2 in Eq. (12). Depending on the Reynolds number, 5 to 15 terms of summation are enough to obtain accurate FA coefficients to within 10^{-6}. All other FA coefficients in Eq. (10) can be calculated without series summation.

The difference between the present finite analytic method and that proposed by Dennis and Hudson [10] is that in the present FA method the exact solution to the linearized partial differential equation for an element is solved and used to formulate the 9-point algebraic equation relating the interior node to the neighboring eight nodes. The boundary conditions used are a combination of three natural solution forms: constant, linear function, and exponential function. On the other hand, the five-point finite difference [10] is derived for a linearized ordinary differential equation along a line. As a result the five-point formulation cannot incorporate the corner points. This, pointed out by Patankar [7], will produce false numerical diffusion if the flow approaches the element from a skew direction. The 9-point finite element formula proposed by Barrett and Demunski [11] was based only on the exponential trial and test functions and the other natural solution forms of the two-dimensional convective transport equation (such as, constant and linear function) used in the FA method are excluded. The stability and accuracy of the finite difference [10] and finite element [11] numerical methods were only tested at $\mathrm{Re} = 400$ in the cavity problem. In the present method Reynolds numbers as high as 2000 in the unsteady cavity problem were tested with good results. The use of separation of variables to obtain the analytic solution seems to be cumbersome, but we found that the results are quite good. Another approximate solution obtained from the collocation was also investigated. The result is less satisfactory since the collocation method required only satisfying the eight discrete boundary nodal values while disregarding the functional behavior between the boundary nodal values.

IV. Starting Flow in Two-Dimensional Cavity

In order to test the FA method we choose a model problem of starting flow in a two-dimensional square cavity ($H \times H$) where the flow starts from rest when the bottom surface of the cavity wall is set to a tangential uniform motion with a speed of U_0. The governing equation for the flow is given in Eqs. (1)–(3). The boundary conditions are $\psi = 0$ and ψ_x (or ψ_y) $= 0$ for stationary wall, and $\psi = 0$, $\psi_y = 1$ for the bottom moving wall. The vorticity boundary condition for Eq. (1), for example, on the left stationary wall $x = 0$, can be obtained from Taylor-series expansion of ψ, or $\xi(0, y, t) = -2\psi(h, y, t)/h^2$. Boundary conditions for the other two stationary walls can be similarly specified. On the moving wall $y = 0$, $\xi(x, 0, t) = -2\psi(x, k, t)/k^2 + 2/k$. The vorticity conditions for the two upper corners are $\xi = 0$, while for the two lower corners they are $\xi = 2/k$. The initial conditions are taken to

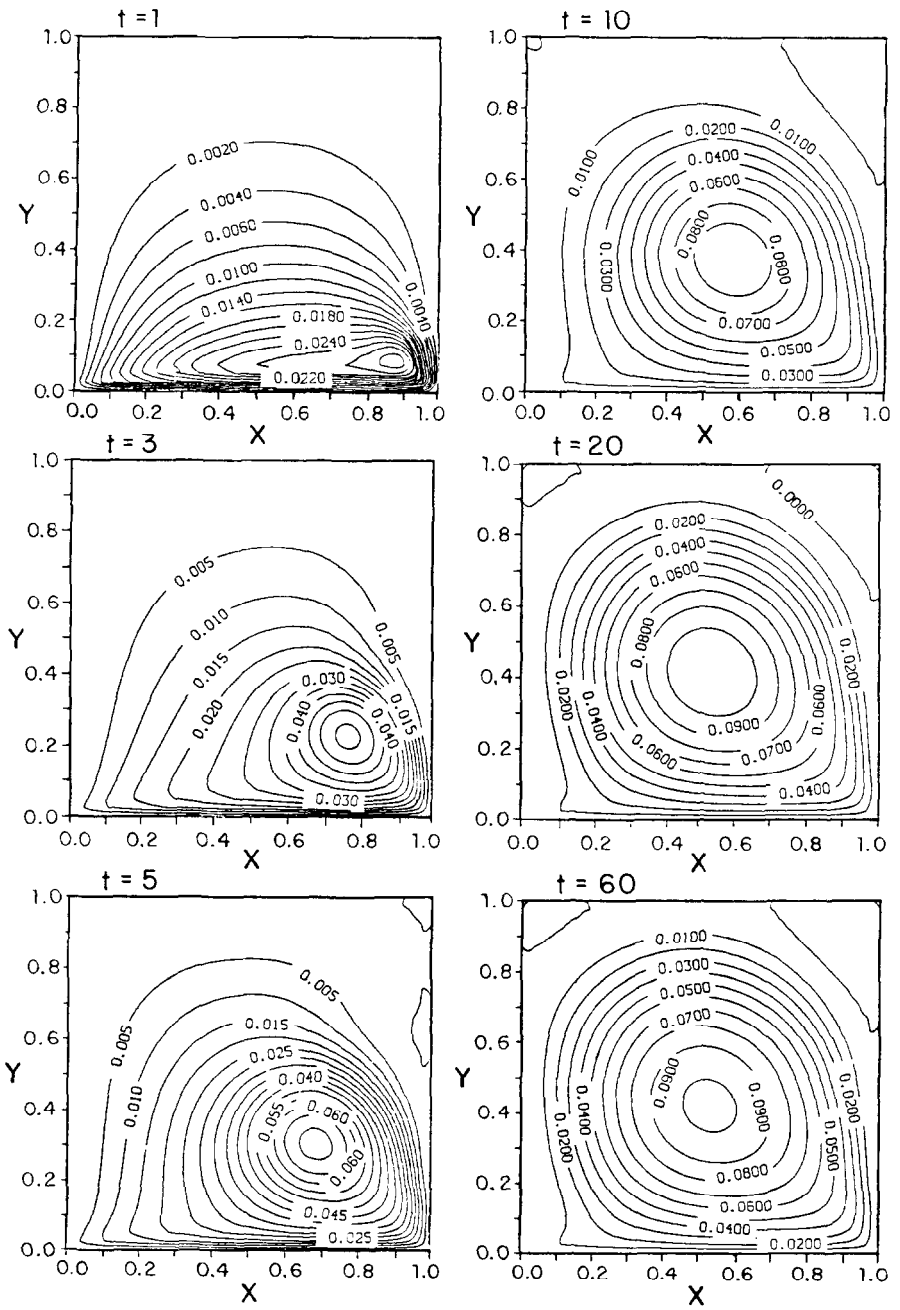

FIG. 2. Evaluation of streamfunction in cavity for Re = 1000.

be at rest or $\psi = \xi = 0$. The numerical solution at the kth time step is obtained by solving Poisson Eq. (2) or Eq. (21) for the stream function first with line-by-line iterations for each time interval. The velocity components u and v are then calculated and substituted into the vorticity transport equation, Eq. (18). With the vorticity boundary conditions evaluated from the stream function just obtained, the vorticity transport equation is solved. Subsequently the correction term F_p in Eq. (18) is tabulated and the computation is repeated for the next time step by solving Eq. (21) again. A time increment of 0.1 is used in the first 200 time steps. Thereafter, a larger time increment of 0.4 is used.

Figure 2 illustrates the FA numerical result for Reynolds number of 10^3 with uniform grid size ($h = 1/40$). The figure shows the time sequence of flow development at $t = 1$, 3, 5, 10, 20, and 30. The flow profile at $t = 30$ and 60 are found to be about the same. At $t = 60$ the maximum stream function $\psi_{\max}$ is 0.1026 and the vorticity at the vortex center is $\xi = 1.896$. The FA solution given here shows that it is stable and accurate and converges rapidly. The large time solution is verified well with previous calculations of Chen *et al.* [3] and many others [12–15] as that shown in Table I. Recently Quartapelle [16] calculated the transcient flow in a two-dimensional square cavity with finite difference scheme and showed that the solution is unstable and the vorticity near the moving surface exhibits a large oscillatory behavior. Quartapelle's calculation was stopped at $t = 15$. This instability phenomenon is not encountered in the present FA solution. In the FA solution the separation of flow at the upper corner appears as early at $t = 5$, but was not predicted by Quartapelle. Figure 3 gives the FA solution for steady streamlines and vorticity lines for Reynolds number of 400, 1000, and 2000. Stable numerical solutions are obtained. Experimentally Pan and Acrivos [17] reported that the transition from laminer to turbulent flow occurs at Reynolds number of approximately 5000.

TABLE I

Comparison of Large Time Cavity Flow Numerical Results for Re = 1000

Reference	Grid	$\psi_{v.c.}$	$\omega_{v.c.}$
[3]	41×41	0.0946	1.62
[12]	81×81	0.1132	2.08
[13]	81×81	0.99	—
[14]	65×65	0.114	1.985
[15]	51×51	0.977	1.83
Present	41×41	0.1026	1.896

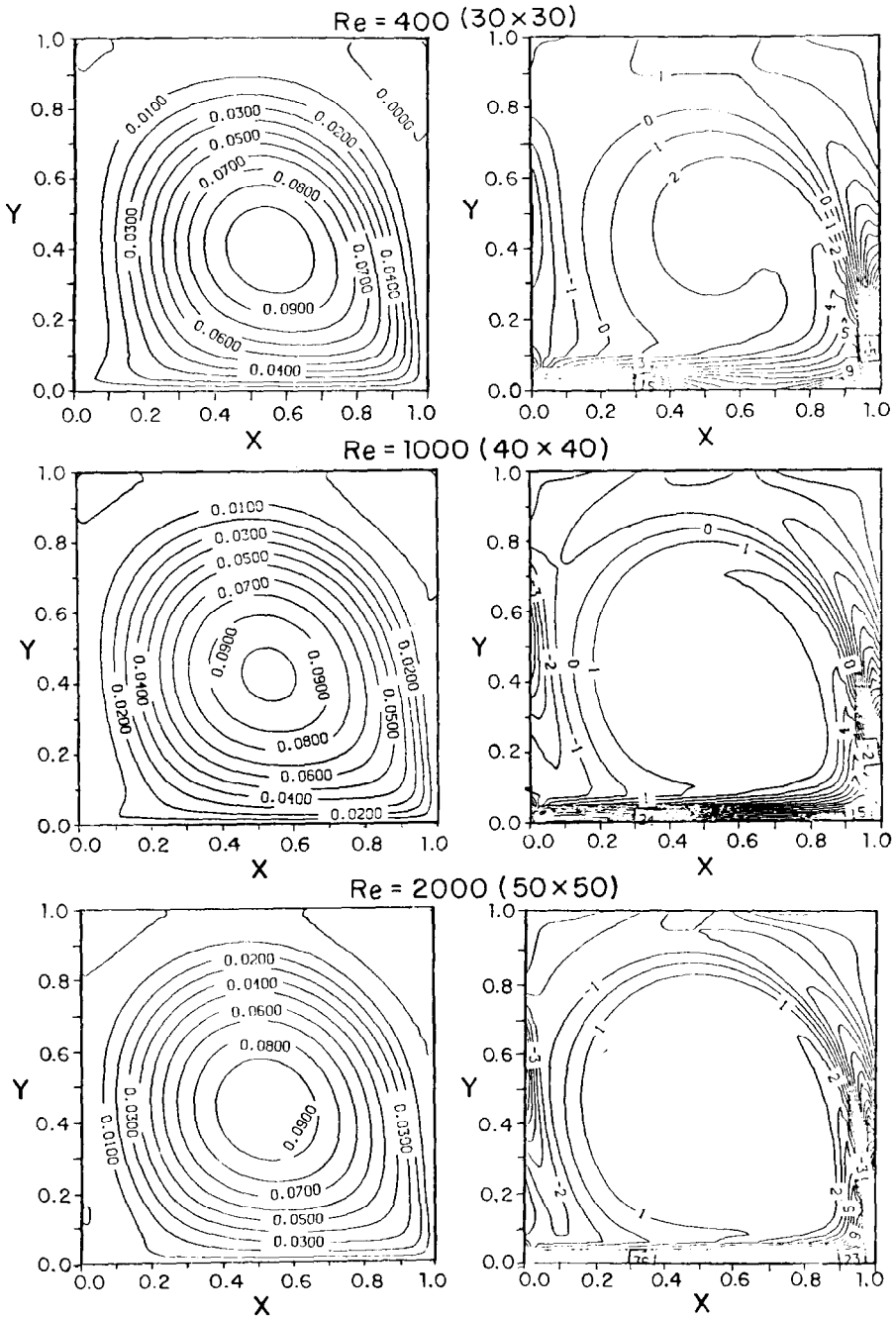

FIG. 3. Streamfunction and vorticity for Re = 400, 1000, and 2000.

V. Vortex Shedding behind an Obstacle

In the next example consider the vortex shedding phenomenon behind a twodimensional rectangular block of $H \times H/4$ when it is placed in a uniform flow of velocity U_0. The computational domain is chosen to be $26H \times 6H$ to approximate the infinite surrounding medium. The block is located $2H$ downstream from the upstream computational boundary, as shown in Fig. 4. The initial vorticity is set equal to zero. The boundary conditions are $\xi = 0$, $\psi = y$ at the upstream and $\xi_x = 0$, $\psi_x = 0$ at the downstream side. The top and bottom boundary conditions are $\xi = 0$, $\psi = +3$ and $\xi = 0$, $\psi = -3$, respectively.

Figures 4–8 give the finite analytic numerical solution for Re = 100, 200, and 500. The computational grid for Re = 100 in x and y direction are set to $h = 0.5$ (3

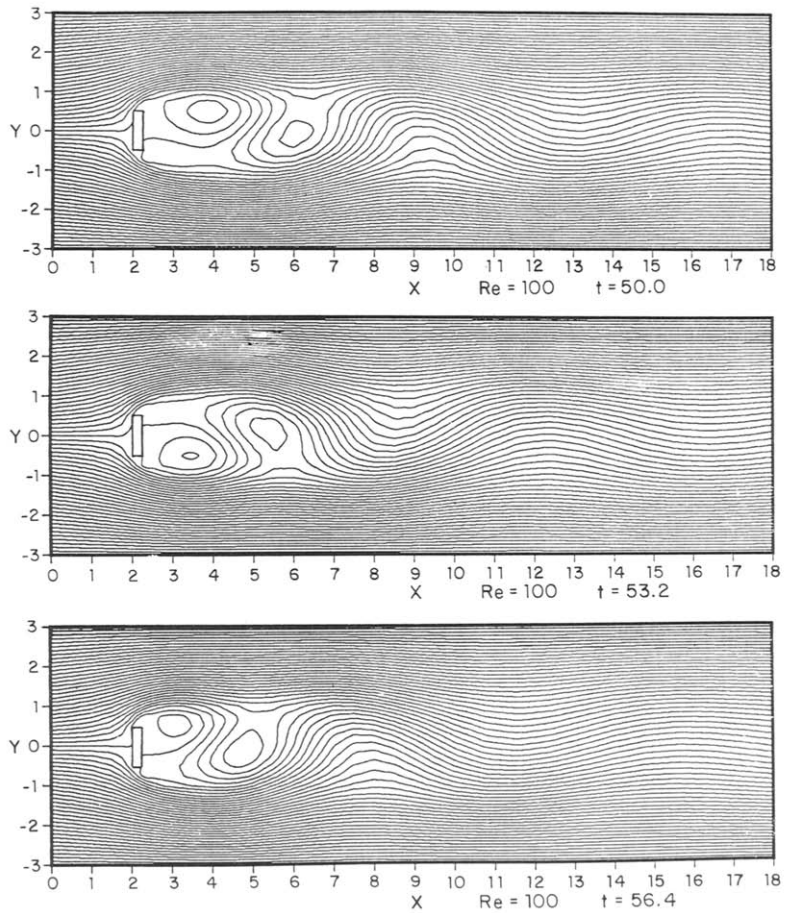

FIG. 4. Streamline for flow over rectangular block (Re = 100).

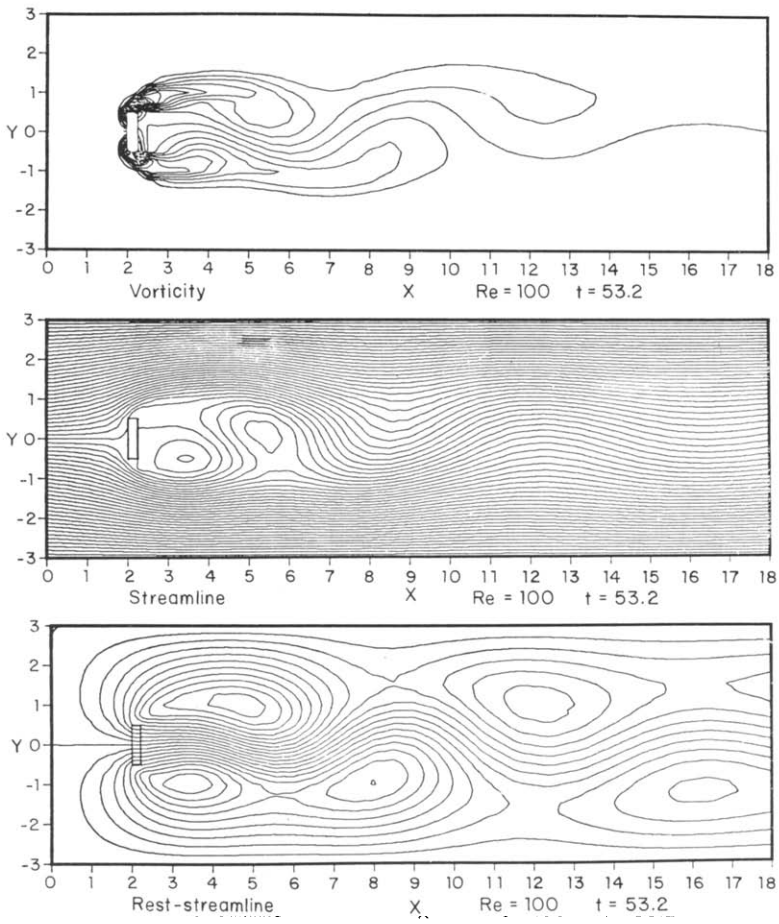

FIG. 5. Vorticity, streamline, and rest-streamline for Re = 100.

nodes), 0.24 (14), 0.5 (10), 0.8 (20), and $k = 0.25$ (24), respectively, for a total of

increment for the initial 40 steps is 0.5, thereafter 0.2. It is found that without artificial perturbation the unsymmetrical flow pattern begins to appear around $t = 30$ behind the block after the transition from the initial zero vorticity field to a symmetric flow of two vortices with similar, but opposite, strength formed behind the block. In the calculation the accuracy for convergence is set $\Delta\psi < 10^{-5}$ and $\Delta\xi < 10^{-5}$ between two iterations. The calculation procedure for each time step is similar to the previous example. Figure 4 illustrates the stream function of vortex shedding which gives the Strouhal number of $S = 0.156$ (i.e., shedding

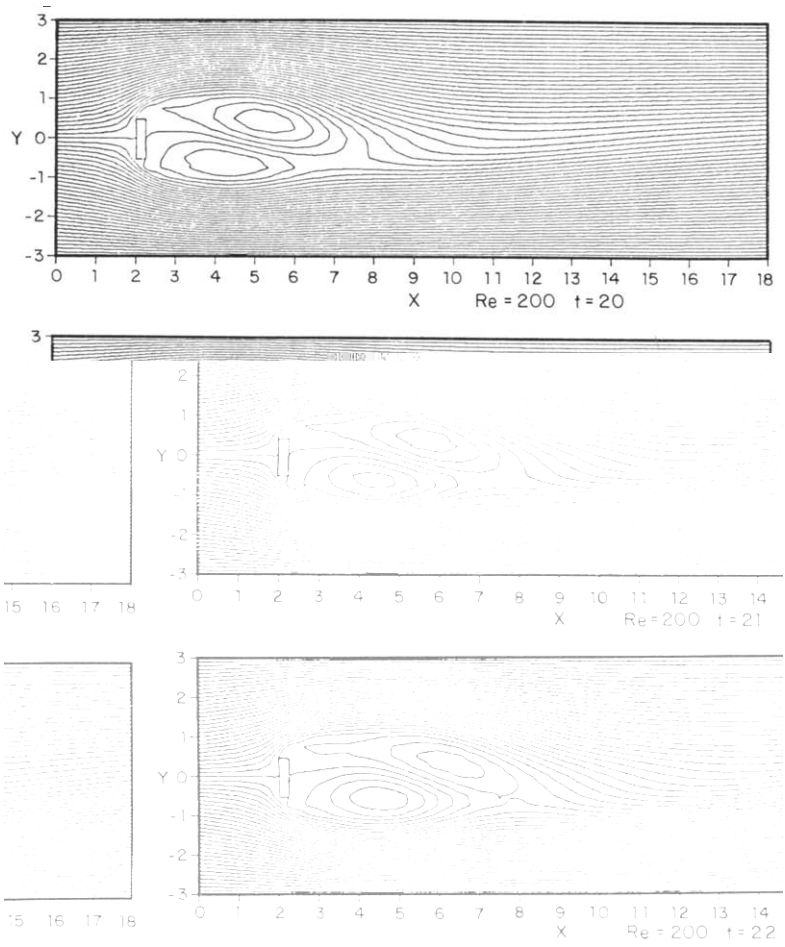

FIG. 6. Streamlines for Re = 200.

frequency $\times H/U_0$). This matches well with experimental measurement of $S = 0.16$ given by Blevins [18] for a similar two-dimensional block.

It should be remarked that because of the unsteadiness of vortex shedding the streamlines plotted on Fig. 4 are not the streak lines that are normally photographed in the experimental visualization. After a vortex breaks off from the block it indeed continues winding. However, the vortex also convects rapidly downstream such that the velocity vector of any fluid in the vortex is all directed toward downstream. This is why no further closed steamline for the moving vortex can be observed in Fig. 4, other than the two vortices sucked behind the block. In order to illustrate the vortex pattern further downstream, the FA numerical solution of stream function, rest-stream function, and vorticity distribution for Re = 100 at $t = 53.2$ is plotted in

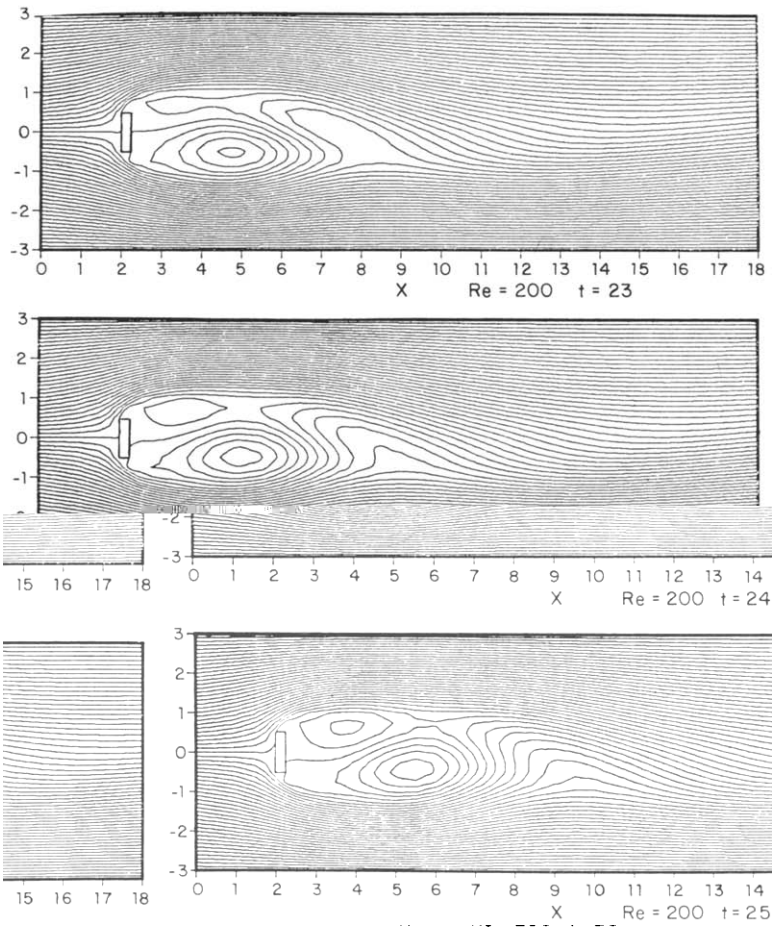

FIG. 7. Streamlines for Re = 200.

Fig. 5. The rest-streamlines are the streamlines as seen by an observer moving with the free stream velocity U_0 toward the block. In this reference frame the ambient fluid appears to be at rest with respect to the observer while the block is seen to be moving from right to left in the figure.

Figures 6–8 show the streamline and vortex shedding phenomena of flow behind the block at a higher Reynolds number of 200 and 500. We note that the vortex shape behind the block at a higher Reynolds number becomes narrower and slim compared to that for Re = 100. The shedding frequency or Strouhal number for Re = 500 is now predicted to be approximately $S = 0.125$ for a shedding period of $t' = 8$, which also correlates well with the experimental measurement of flow over a block with sharp front edge by Blevin [18]. It should be noted here that at Re = 500

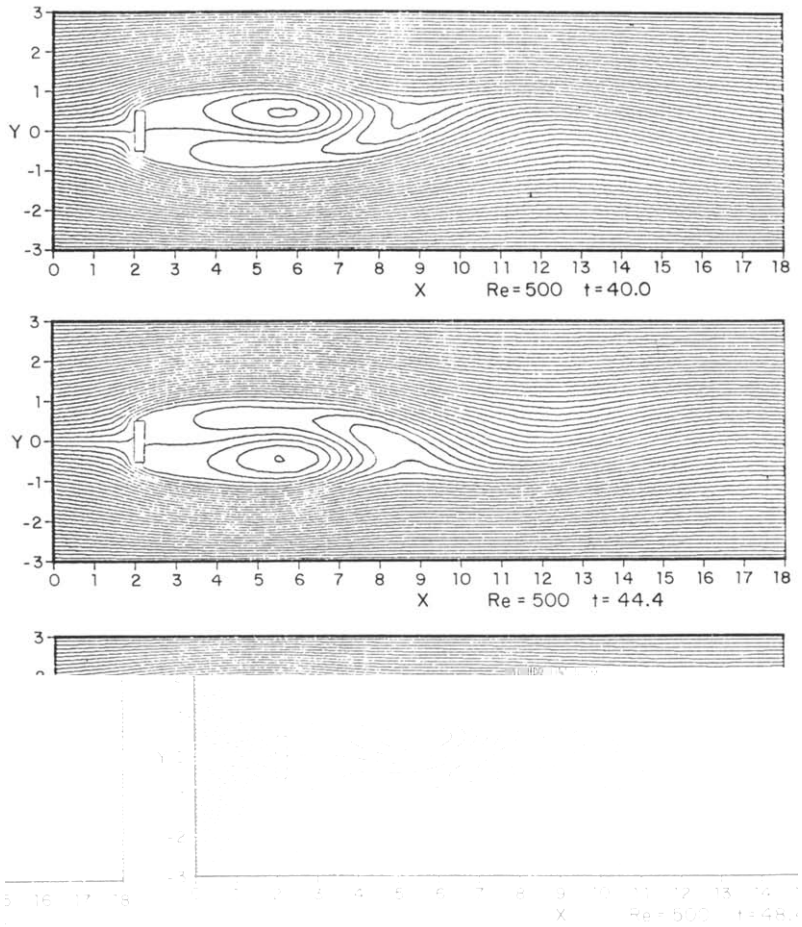

FIG. 8. Streamlines for Re = 500.

the flow is either at the brink of transition or in the transition range. However, the experimental observation shows that the shedding frequency evolves slowly from laminar flow to transition. The Strouhal numbers for various noncircular sections compiled by Blevins [18] at much higher Reynolds numbers of 10^4 or 10^5 still fall between 0.12 to 0.16.

It should be remarked here that analytic solutions for various vortex shedding immediately behind the block are difficult, if not impossible to obtain. Fromm and Harlow [19] attempted to solve numerically the vortex shedding phenomenon behind a series of rectangular blocks in a channel by the finite difference method. In their calculation a periodic boundary condition is used, i.e., the upstream and downstream boundary conditions are set equal to each other. They reported that an artificial

perturbation of vorticity is needed to trigger the vortex shedding. In the present investigation a single block is considered, hence, the periodic boundary condition is not used. Nor in the present study is an artificial perturbation required to trigger the vortex shedding. Smith and Brebbias [20] computed the vortex shedding behind a thick block with the finite element method and reported that, due to the inherent instability of the explicit time integration method used in the finite element formulation, the time step must be kept very small. For $Re = 100$ the time increment used is 0.03. In the present calculation the time increment of 0.5 or 0.2 was used. Indeed a larger time step can be used in the FA method.

VI. Conclusion

The finite analytic solution for the unsteady two-dimensional transport equation is derived. For every element a 9-point FA algebraic equation is obtained from the analytic solution of locally linearized transport equation with the element boundary function approximated by a combination of linear and exponential functions. The FA solution predicts the starting cavity flow, that the vortex begins to form near the downstream side of the moving boundary, and gradually moves to the center of the square cavity. The secondary vortex first appears at the downstream stationary wall. The FA solution predicts the vortex shedding phenomena in the region behind a rectangular block. The predicted Strouhal numbers of 0.156 and 0.125 for Reynolds number of 100 and 500, respectively, correlate well with experimental measurement.

The finite analytic solution is shown to properly describe the influence of convection on the solution for fluid flow from low to high Reynolds number. Furthermore, it is found that the finite analytic solution is stable at all Reynolds numbers investigated and converges rapidly.

Acknowledgments

This research is in part supported by NASA Grant NSG 3305 and DOE Grant DE-AC02-79ER-10515.A000.

References

1. C. J. Chen and P. Li, "Finite differential method in heat conduction—Application of analytic solution technique," ASME *Paper*, 79-WA/HT-50, December 2-7, ASME Winter Annual Meeting, New York, 1979.
2. C. J. Chen and P. Li, "The finite analytic method for steady and unsteady heat transfer problems," ASME Paper, 80-HT-86, 1980.
3. C. J. Chen, H. Naseri-Neshat, and K. S. Ho, Finite analytic numerical solution of heat transfer in two-dimensional cavity flow, *in* ASME HTD Vol. **13**, "Momentum and Heat Transfer Processes in Recirculating Flows" (B. E. Launder and J. A. C. Humphrey, Eds.); *J. Numer. Heat Transfer*, **4** (1981), 179.

4. C. J. CHEN AND K. OBASIH, Finite analytic numerical solution of heat transfer and flow past a square channel cavity, *in* "The 7th International Heat Transfer Conference, Munich," 82–IHTC–43. September 6–10, (1982).
5. P. J. ROACHE, "Computational Fluid Dynamics," Hermosa Pub., Albuquerqe, N. Mex., 1972.
6. D. B. SPALDING, *Int. Numer. Methods Eng.* Vol **4** (1972), 551.
7. S. V. PATANKAR, "Numerical Heat Transfer and Fluid Flow," McGraw–Hill, New York, 1980.
8. J. C. HEINRICH, P. S. HUYAKORN, O. C. ZIENKIEWIEZ, AND A. R. MITCHELL, *Int. J. Numer. Methods Eng.* **11** (1977), 131.
9. R. H. GALLAGHER, J. T. ODEN, C. TAYLOR, AND O. C. ZIENKIEWIEZ, "Finite Elments in Fluids," Vol. 3, p. 1, Wiley, New York, 1978.
10. S. C. R. DENNIS AND J. D. HUDSON, *J. Inst. Math. Its Appl.* **26** (1980), 369.
11. K. E. BARRETT AND G. DEMUNSKI, *Int. J. Numer. Methods Eng.* **14** (1979), 1511.
12. W. A. SHAY, *Comput. Fluids* **9** (1981), 279.
13. A. D. GOSMAN, W. M. PUN, A. K. RUNCHAL, AND D. B. SPALDING, "Heat and Mass Transfer in Recirculating Flows," Academic Press, New York/London, 1969.
14. S. G. RUBIN AND P. K. KHOSLA, *J. Comput. Phys.* **24** (1977), 217.
15. M. NALLASAMY AND K. K. PRASAD, *J. Fluid Mech.* **79** (2) (1977), 391.
16. L. QUARTAPELLE, *J. Comput. Phys.* **40** (1981), 453.
17. F. PAN AND A. ACRIVOS, *J. Fluid Mech.* **28** (4) (1967), 653.
18. R. D. BLEVINS, "Flow-induced Vibration," Chap. 1, Van Nostrand–Reinhold, Princeton, N. J., 1977.
19. J. E. FROMM AND F. H. HARLOW, *Phys. Fluids* **6** (7) (1963), 975.
20. S. L. SMITH AND C. A. BREBBIAS, *J. Comput. Phys.* **17** (1975), 235.